DETERMINATION OF THE AERODYNAMIC RESISTANCE TO HEAT USING MORPHOMETRIC METHODS

Corinne M. Frey, and Eberhard Parlow

University of Basel, Switzerland; corinne.frey(at)freenet.ch, eberhard.parlow(at)unibas.ch

ABSTRACT

The spatial estimation of the aerodynamic resistance to heat using morphometric methods was evaluated on the example of three different approaches using a digital surface model to calculate the roughness length for momentum and heat. The digital surface model was a result of manual digitising of a GoogleEarth image and another model retrieved from two stereoscopic SPOT images. The resulting values for the building area density and frontal area index were slightly lower than comparable values found in the literature, which could be attributed to the building structure. An empirical parameter α, used for the calculation of the roughness length for heat, was fitted to observational data. α was found to be higher than suggested by literature values. The three morphometric methods proved to follow the same principle, the spatial analysis, however, showed that they produced different results in some very dense areas.

INTRODUCTION

The determination of the aerodynamic resistance to transfer of sensible heat r_h, short 'aerodynamic resistance to heat', is necessary in the estimation of heat fluxes using bulk transfer methods applied with satellite data. In such approaches, remotely sensed surface temperatures are combined with an estimation of this parameter r_h, together with the climatological variables air temperature, net radiation, and soil heat flux to derive the final product, the turbulent heat fluxes. r_h thereby is a function of the roughness of the surface, described by the displacement height z_d and the roughness length for momentum z_{0m} and heat z_{0h} (1). The roughness of the surface is very distinct in urban areas; therefore a sound determination of these parameters is essential for successful flux modelling. Several morphometric methods have been summarised in (2) to determine z_d and z_{0m} from a digital surface model, finding a distinct variability in the output of the tested approaches. They ranked the approaches by comparing their output to measurement values. They found the methods presented in (3,4,5,6) to score highest. Liu et al. (7) also verified these three methods with observational data. Their results suggest that the three methods are not very different from each other.

In the above-mentioned three morphometric methods, the average roof height, the building area density, and the frontal area index are used. These indices can be calculated from a digital surface model using trigonometry. The calculation of these parameters in a GIS (Geographic Information System) and their subsequent use for the estimation of the roughness parameters is described in (8). Also some other studies have reported on roughness parameters in urban areas. In (9), for example, is presented an urban roughness mapping method with the approach from (3) to localise ventilation paths in the city. (10) used the approach from (6) to extract several flow and dispersion parameters from an urban database. The parameters are the plan and frontal area densities, their function and distribution with height, their standard deviation, the aerodynamic roughness length and the sky view factor. (11) finally compared the methods of (3) and (4,5) for a portion of Rome, using cadastral databases. In many developed countries, digital surface models have been made available for cities by the respective authorities. In developing countries, however, this data is mostly not existing at all or not available for external researchers. For our study area, too, there was no such model available; therefore it had to be generated manually. The resulting digital surface model does not offer the same accuracy of up-to-date models generated from cadastral maps and provided by authorities. However, it is a good alternative and is sufficient for the needs of this study.

In this research, the three above mentioned best-fitting morphometric methods for the estimation of z_d and z_{0m} are used to deduct the aerodynamic resistance to heat r_h for a comparison with estimations of r_h from *in situ* measurements in an urban area. The methods used were proposed in (4-6,3) and are further referred to as RA, MA and BO. Additionally, an empirical relation connecting the roughness length heat z_{0h} with Re^* (12,13) was fitted to the data set with in situ measurements of r_h. A new value of an empirical parameter used in this relation is subsequently proposed.

The results of this study can be used by researchers using very high resolution remote sensing approaches or urban climate models, by seeing the effect of these three different approaches and by proposing a new empiric value for the estimation of the roughness length for heat in urban areas. Especially the definition of new values for this relation has been the topic of a couple of recent publications (13,14,15) which focus on urban environments. This research is further input in this discussion. Besides this, the study shortly discusses the optimal resolution for the calculation of the input parameter from the digital surface model for this study area.

STUDY AREA

The study area is a small part of the Gizah district in the megacity Cairo in Egypt: the campus of the Cairo University in the centre of the area. The campus consists of broad blocks and spacious squares and alleys. Some trees and bushes are planted along the alleys. Botanical test fields are to the south of the campus. The fields of this area are sometimes surrounded by trees. A park and a zoological garden both with dense tree cover are found in the east of the campus and very dense housing blocks emerge from the west and to the north of the campus. These blocks belong to lower income social classes. The cross-streets between the single houses of these blocks are extremely narrow and often are not clearly detectable on satellite images. The whole area is 3.205 km $\times$ 2.45 km.

METHODS

Calculation of the aerodynamic resistance to heat

From November 2007 to February 2008 a micrometeorological field campaign was conducted in Cairo, Egypt (16). Micrometeorological parameters were continuously measured at three stations. One of these stations was located at the campus of Cairo University, on a building in the south of the campus ('Laser'-Building at 30°01'33.39''N, 31°12'27.81''E, see Figure 1). According to (1), r_h (given in s m^{-1}) was computed from measurements of radiative surface temperature T_s, air temperature T_a and sensible heat flux Q_H in half hourly intervals.

$$r_h = \rho_{air} \cdot C_p \cdot \frac{T_s - T_a}{Q_H} \tag{1}$$

where ρ_{air} is the density of air and C_p the specific heat of air at constant pressure.

Also following (1), r_{ah} can be expressed by

$$r_{ah} = \frac{1}{ku^*}\left(\ln\left(\frac{z - z_d}{z_{0m}}\right) - \psi_h\right) + \frac{1}{ku^*}\ln\left(\frac{z_{0m}}{z_{0h}}\right) \tag{2}$$

as was done previously by (17). u^* is the friction velocity, k is Karman's constant (k = 0.4) and ψ_h is a stability correction function for heat, depending on the Monin Obukhov length (18).The first term in Eq. (2) thereby corresponds to the aerodynamic resistance for momentum, the latter term to a bulk aerodynamic excess resistance. Please refer to (7) for other parameterisations of r_{ah}. As Eq. (2) does not allow an input of zero for z_{0m} and z_{0h}, these terms were set to 10^{-4} and 10^{-5} in respective cases.

The aerodynamic surface temperature T_0 which is originally used in the bulk transfer equation (Eq. 1) is the temperature extrapolated to a surface that is at the height z_d + z_{0h} (the zero-plane displacement length plus roughness length for heat). However, the introduction of a corrective

term, the radiometric excess resistance, allows substituting T_0 with the radiometric surface temperature T_s as was done in Eq. (1) (19). The radiometric excess resistance is:

$$r_r = \frac{kB^{-1}}{u^* k}, \tag{3}$$

with

$$kB^{-1} = \ln\left(\frac{z_{0m}}{z_{0h}}\right) \tag{4}$$

r_h in Eq. (1) is given by:

$$r_h = r_{ah} + r_r \tag{5}$$

Please refer to (20) for a more detailed discussion of the assumptions made above.

The roughness length z_{0m} used in Eq. (2) was estimated with the three methods RA, MA and BO. All these methods need the input parameter λ_f which is the frontal area index. This index uses the length of any obstacle, the mean height of the obstacle, as well as the angle of attack of the prevailing wind to the obstacle in a given window. To extract this information for the given area, a digital surface model must be available. As no such model was available for the study area, it was generated manually as described in the next section.

Generation of a digital surface model

For the calculation of the roughness lengths, a simple digital surface model of the closer surrounding of Cairo University was built at first. The buildings were digitised manually from a GoogleEarth cut-out in 1.5 km view in the ENVI programme (ITT Visual Information Solutions). Many of the cross-streets in some low income areas were not detectable from the Google Earth image. Therefore, the houses along a bigger street were digitised as one block. These cross-streets are extremely narrow and the wall surfaces of the canyons are not exposed to the dominant wind system of the broader area. Therefore it is considered to be legitimate to omit these streets and treat the building series of a whole street-side as one block. Afterwards, mean heights were allocated to the buildings using a coarser digital surface model of the area that was extracted from two stereoscopic SPOT images (21). As the SPOT surface model did not assign a correct height to the 'Laser'-Building, a corrective factor was introduced all over the area to match the height of the 'Laser'-Building to the actual height of the building.

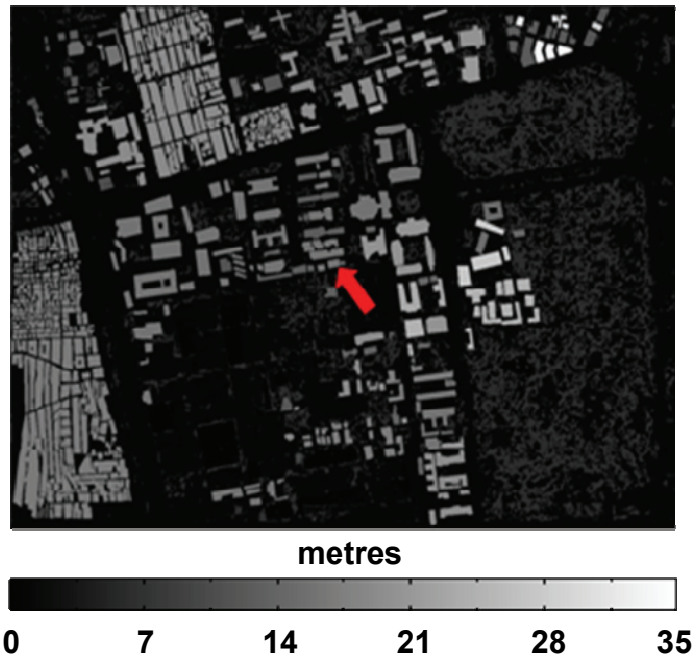

Figure 1: The surface model including vegetation. Grey values correspond to height. The model is oriented to north.

Some extended vegetated areas exist in the area as described above. To analyse the influence of this vegetation on the estimated roughness parameters, a second model was built. Trees and fields were extracted using the RGB values of the Google Earth image. Thereby thresholds for the slope between the blue and the green and between the green and the red channel were used to find the vegetated areas. Trees and fields were then separated using the dissimilarity filter implemented in the ENVI programme. The vegetative covers of the fields were assigned a height of 0.2 m; trees got an average height of 8 m. By merging the two height models – buildings and vegetation - a second model was built. Figure 1 shows this model in 2D. Both models were saved with a spatial resolution of 2.5 m.

Estimation of the frontal area index λ_f

There is no common way of calculating the frontal area index so far, thus the used routine shall be explained below. In a first step, the length of any obstacle in a moving window was calculated. The window width was 3 pixels (corresponding to 7.5 m). Therefore, it was assumed that only one obstacle can be located in the set window at any time (Figure 2).

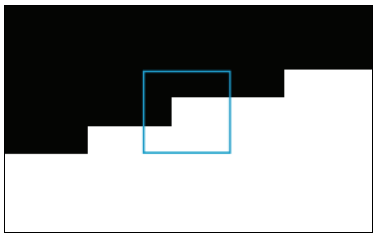

Figure 2: Example of a south-south-east oriented wall with a moving window size of 3 pixels (blue square). Inside the moving window there are 4 black pixels representing an obstacle and 5 white pixels representing open space.

In each window, the pixels were divided into obstacle and open space. If one of the four direct neighbouring pixels of a pixel was open space, then this pixel was classified as wall (belonging to an obstacle). The boundary of this obstacle (building or a group of trees) could have only one direction (azimuth angle, east of north). Edges of obstacles were not detected separately. So, if an edge occurred in the window, it was treated as a wall, having the directional properties of the mean of the two adjacent walls of the edge. The mean azimuth angle of all wall pixels was determined using trigonometry. The mean height is just the average height of all obstacles in a window.

This approach was originally developed for buildings only. Vegetation in the second model is handled in the same way as buildings. This simplification introduces some uncertainty, as vegetation is semi-permeable for air masses and does not cause the same roughness as massive walls. The inclusion of vegetation might therefore overestimate the roughness, and results should be treated with care.

The calculations of the frontal area index λ_f and the density of the obstacles λ_p were done in a second step with a moving window of 125 m (50 pixels). λ_f was calculated using

$$\lambda_f = \frac{\overline{L_y}\,\overline{z_h}}{A_T} \tag{6}$$

where $\overline{L_y}$ is the mean breadth of roughness elements perpendicular to the wind direction. The mean breadth of the roughness elements was weighted with a cosine function according to the relation of the azimuth angle and the angle of attack of the wind. $\overline{z_h}$ is the mean height of the lot area and A_T is the total lot area. The density of the obstacles λ_p, used for example in Eq. (7), was estimated using the ratio of the number of pixels with obstacles and the window size.

It has been pointed out in (8) that the window size for the calculation of λ_f should be chosen such that the characteristics of interest in the urban area are discernible. In this research, the window

size for the calculation of the frontal area index was first varied from 25 m to 150 m to assess the sensitivity of r_h to the window size. It was found that window sizes greater than 75 m produced r_h values that did not change anymore significantly. Lower window sizes, however, increased r_h substantially. For example: r_h calculated with a 25 m window size was 20 to 40 sm^{-1} lower than calculated with a 150 m window size (MA method with α ranging from -0.1 to -1, see Eqs. (9), (10) and (14), including all occurring wind speeds). Lower α values decrease the difference. Further analyses are made on 125 m basis, which is thought to be a good window size to represent a single unit in this study area, coupled with acceptable computing times. Smaller sizes down to 75 m would also be acceptable. Larger window sizes (in this study done up to 150 m) are just increasing the computing time.

Calculation of roughness lengths

The roughness lengths were then estimated following the three approaches addressed in the introduction. BO relates z_d/z_h to an exponential curve of the density of the obstacles λ_p, while z_{0m}/z_h is given by a natural logarithm. For simplicity, the in-plane sheltering displacement height of BO is set equal to z_d:

$$\frac{z_d}{z_h} = \lambda_p^{0.6} \tag{7}$$

$$\frac{z_{0m}}{z_h} = \frac{z_h - z_d}{z_h} \exp\left(-\frac{k}{\left(0.5 C_{Dh} \lambda_f\right)^{0.5}} \right) \tag{8}$$

C_{Dh} is the isolated obstacle drag coefficient (C_{Dh} = 0.8). According to MA, the zero-plane displacement height z_d is given by:

$$\frac{z_d}{z_h} = 1 + \alpha_m^{-\lambda_p} \left(\lambda_p - 1\right) \tag{9}$$

The roughness length for momentum z_{0m} is found by:

$$\frac{z_{0m}}{z_h} = \left(1 - \frac{z_d}{z_h}\right) \exp\left(-\left[0.5 \beta_m \frac{C_D}{k^2} \left(1 - \frac{z_d}{z_h}\right) \lambda_f \right]^{-0.5} \right) , \tag{10}$$

where α_m and β_m are empirical constants. The latter constant is a net correction factor for the drag coefficient. Recommended values are α_m = 4.43 and β_m = 1.0. C_D is a drag coefficient (C_D = 1.2).

RA gives the zero-plane displacement height z_d as

$$\frac{z_d}{z_h} = 1 - \frac{1 - \exp\left(-\left(2 c_{d1} \lambda_f\right)^{0.5}\right)}{\left(2 c_{d1} \lambda_f\right)^{0.5}} \tag{11}$$

and the roughness length for momentum z_{0m} is found by

$$\frac{z_{0m}}{z_h} = \left(1 - \frac{z_d}{z_h}\right) \exp\left(-k \frac{U}{u^*} + \psi_h \right) \tag{12}$$

where

$$\frac{u^*}{U} = \min\left[\left(c_s + c_r \lambda_f\right)^{0.5}, \left(\frac{u^*}{U}\right)_{\max} \right] \tag{12}$$

ψ_h is the roughness sublayer influence function, U is the large-scale wind speed, u^* is the friction velocity, c_s and c_r are drag coefficients for the substrate surface at height z_h in the absence of roughness elements, and of an isolated roughness element mounted on the surface. c_{d1} is an empirical constant. According to RA c_S = 0.003, c_R = 0.3, $(u^*/U)_{max}$ = 0.3, ψ_h = 0.193, and c_{d1} = 7.5 were used. Note that the notation of Eq. (11) is different from the respective one given in (2).

The roughness length for heat z_{0h} was found for all three approaches using

$$z_{0h} = z_{0m}\beta \exp\left(\alpha \; Re^{*^{0.25}}\right) \tag{13}$$

with *Re** being the Roughness Reynolds number. α and β are empirical constants for bluff-rough situations given by (12). (17) and (15) used α = -1.29, which they took from the work of (13) for urban areas. (13) regressed data from an outdoor experiment with the Comprehensive Outdoor Scale Model (COSMO) to find the relationship between kB^{-1} and *Re**, a different form of Eq. (14). They found that the regressed function agreed better with the data from three other urban sites than using the value in (12), even though the surface geometry of the urban sites differed. This α parameter is subject to further research in this paper and alternative values are investigated. β is kept constant at 7.4 (20).

To give an overview of the whole methodology, a diagram with an overview of the different processing steps in this study is given in Figure 3.

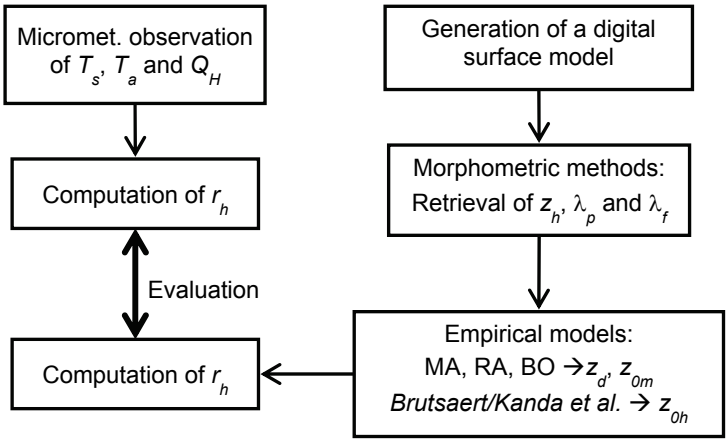

Figure 3: Overview of the different processing steps of the study

Footprint modelling

To compare the results with the measurements, the footprint model of Kormann & Meixner (22) was used. The model output was thereby adjusted to the pixel resolution of the city model and laid over the image to fit the location of the measurement station.

RESULTS

Mean density and frontal area index

The mean density λ_p and the mean frontal area index λ_f were calculated in two ways: a) for the whole area and b) for only the built up area, excluding the botanical test fields in the south of the campus and the parks in the east. This was done for both surface models, excluding and including vegetation. The resulting values are given in Table 1. λ_p ranges from 0.170 to 0.413, λ_f from 0.079 to 0.138. This corresponds to the lower range of the values of λ_p and λ_f given in (2).There, λ_p ranges from 0.33 to 0.58 and λ_f from 0.13 to 0.33. Reasons for our low values are firstly found in the very high density areas, where the buildings are put together in the model to form one big block and secondly in the spacious architecture of the campus.

Table 1: Mean density λ_p and mean frontal area index λ_f as calculated from the 125 m resolution windows.

	z_h	λ_p	λ_f
1. First model (including only buildings)			
Whole area	9.21	0.170	0.079
Built up area only	12.72	0.256	0.117
2. Model (including also vegetation)			
Whole area	8.09	0.413	0.104
Built up area only	10.38	0.346	0.138

Comparison of morphometric methods

In a first step, z_d/z_h, z_{0m}/z_h and z_{0h}/z_h of the three different models (MA, BO and RA) were compared by plotting them against λ_p or λ_f (Figure 4). The relation between z_d/z_h and λ_p is comparable in all three approaches a), d) and g). Especially the curves of MA and of BO are very similar. z_d/z_h increases when the building density is higher. Note that the RA approach relates z_d/z_h to λ_f (black curve). The grey values in Figure 4, however, give the relation to λ_p.

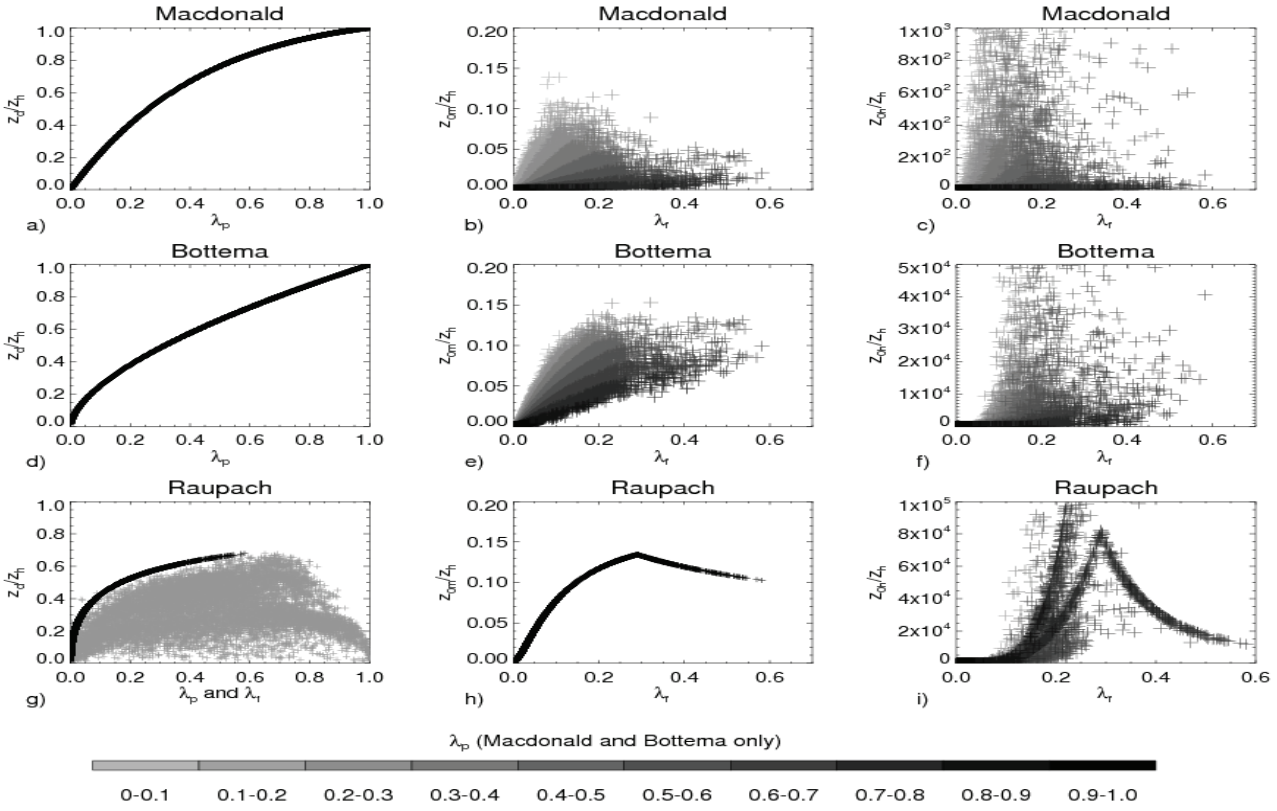

Figure 4: Relation between z_d/z_h and the housing density λ_p and z_{0m}/z_h and z_{0h}/z_h and the frontal area index λ_f for α = 0.8 given for the model including vegetation and a window size of 150 m. b), c) e) and f) show additionally the dependence on λ_p (grey values). Note that h) and i) only show relations to λ_f.

Increasing the housing density continuously, one will reach a point where the roughness peaks at a maximum value. More dense housing will decrease the roughness again, as the narrow canyons lose their influence on the air flow. This fact is depicted in Figures b), e) and h) of Figure 4. All three approaches let z_{0m}/z_h increase by increasing λ_f up to a maximum value, to decrease again. The curve of RA for z_{0m}/z_h is a single curve, as it is only dependent on λ_f, while the curves of MA

and BO are dependent on λ_f and λ_p. The grey values in b) and c) in Figure 4 depict these dependencies and relative λ_p values are given in the scale bar.

The relation between z_{0h}/z_h and the frontal area index λ_f is less clear and subject to strong scattering. Both the approaches from MA and BO have very low values, with a high scattering up to single values around 200'000. The data using the RA approach is following an increasing trend with increasing λ_f.

Alpha parameter

Eq. (14) calculates z_{0h} from z_{0m} and the Reynolds number Re^* using the empirical parameters α and β. (12) sets α = -2.46 for bluff-rough surfaces. However, it seems that this parameter is not suitable for urban areas. While retaining the β parameter of (12),several options for α were investigated. Thereby r_h was calculated iteratively using Eq. (2) with an increasing α. The resulting r_h values, calculated for four wind directions and three wind speed classes, were compared to the r_h values retrieved from the in situ measurements using Eq. (1). It was shown that the wind speed did not influence significantly the retrieved best fitting value. Table 2 gives the differences of the two r_h values respective to α as weighted means from all wind speed classes. It shows that the best fitting α values range from -0.5 to -0.7 for both surface models. These values are higher than the value proposed in (13), but fit much better to the field data shown in (12), Figure 6. Their proposed curve lies mostly over the in situ test data of the business district of Tokyo and the dense residential area of Tokyo, while the curve with the new α values would go right through the measurement data.

In the following several influences in the retrieval of r_h will be investigated. One source of error in the estimation of r_h is the correction of the surface temperatures from the emissivity effect. The emissivity was set to 0.96, according to an analysis of ASTER data of the area (Frey et al. subm.). Comparison calculations showed that lowering the emissivity about 0.02 from 0.96 to 0.94 would decrease the best fitting α values only about 0.1. This quite low difference shows that the emissivity effect alone cannot explain the differences of α to the value in (13) or (12). Another uncertainty is resulting from the fact that instead of the aerodynamic surface temperature T_0 the radiative surface temperature T_s is used in Eq. (1). Despite the use of a corrective term r_r some uncertainty remains, as the departure of the aerodynamic temperature from the radiative temperature is controlled by several factors that cannot be simply put into one corrective term (19). Further, the *in situ* sensor does not sense the complete surface, but only the surfaces in the field of view (20). Vertical walls not seen by the sensor do contribute to the sensible heat flux, but are not included in the measurement. However, assuming that those vertical walls are at least partly shaded and exhibit lower surface temperatures than the roof areas, resulting r_h values would be lower. Such lower r_h would need higher α values to fit the observational data. So, thermal anisotropy is not able to explain the high α values compared to (12), either. The fact, finally, that the λ_p and λ_f values are lower than literature values does not explain this difference either, as higher λ_p and λ_f values would result in a higher aerodynamic resistance to heat, which would also ask for an increase in α to optimally fit the modelled data and the values retrieved from the *in situ* measurements. As a conclusion new α values of -0.5 to -0.7 are proposed for the application in urban areas similar to our Cairo test case.

Figure 5 shows a comparison of the *in situ* measured and modelled r_h values according to the wind direction. Only situations with wind speed greater than 1 ms^{-1} and lower than 7 ms^{-1} are considered. Mean *in situ* values are plotted as bold crosses. They show a distinct directionality which corresponds to the building density in the surrounding of the measurement mast. The modelled values generally follow this pattern well. They were calculated with mean input variables associated with the considered wind speed range. In eastern wind situations the agreement seems to be relatively good, however, not much reference data is available in this sector (23). In western wind situations, r_h is underestimated by all models. Such discrepancies can be attributed to the limited accuracy of the digital surface model and the crude assumptions about vegetation. Note that the *in situ* measured values have a quite high statistical spread.

Table 2: Differences of r_h (sm^{-1}) in a moving window of 125 m. The footprint model of (22) was used for the comparison.

α	BO		MA		RA	
	Buildings	Buildings + vegetation	Buildings	Buildings + vegetation	Buildings	Buildings + vegetation
-0.4	23.39	37.63	14.37	26.99	30.04	44.20
-0.5	9.45	22.54	-1.03	14.68	17.39	30.30
-0.6	-4.44	7.47	-16.36	2.39	4.83	16.48
-0.7	-17.80	-7.56	-30.89	-9.77	-6.86	3.10
-0.8	-29.31	-22.32	-42.85	-21.51	-17.18	-9.65

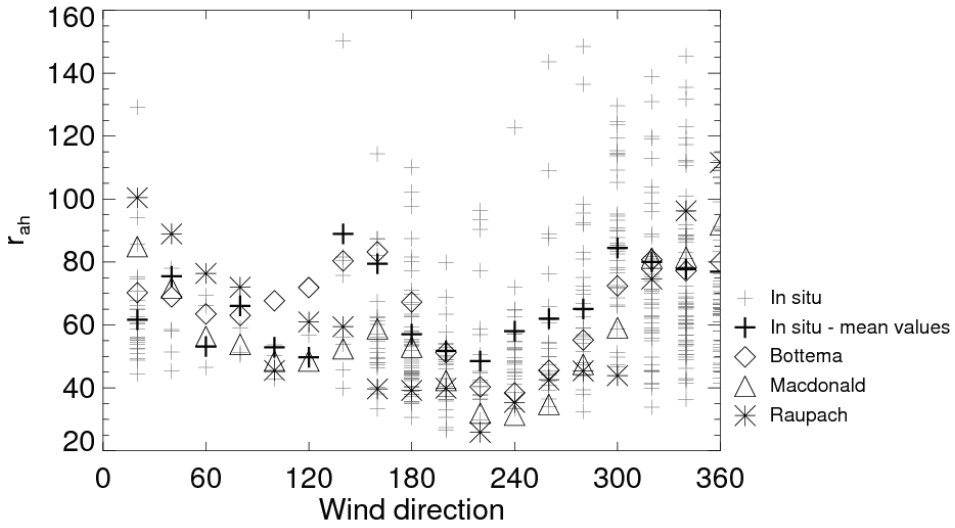

Figure 5: Aerodynamic resistance to heat, calculated with 125 m windows for all wind directions, for the MA, the BO and the RA approach and corresponding in situ values.

Spatial distribution

Extended areas with no significant roughness elements came out with a value of zero for z_{0m} and z_{0h}. These areas were set to 10^{-4}, and 10^{-5} m, respectively. Due to this assumption large areas of the first model with parks and fields (in the east of the image), had a constant r_h value (44 sm^{-1} in Figure 6). The same areas produced values in a similar range in the second model (including vegetation), which is in accordance with the measurements done by (24). The r_h values of the open areas did not influence the estimation of the best-fitting α value, as the footprint rarely extended to the east.

The BO and the RA approaches produced very similar spatial pattern, while the MA approach sometimes behaved inverse to the other two: in the very dense housing areas the MA approach showed lower values than BO and RA (see Figure 6). This difference is due to very low z_{0m} values estimated by the MA approach. The relation of z_{0m} and λ_f can be seen in Figure 4. Furthermore, the MA approach can be distinguished by the production of low z_{0m} values. The MA approach is using two empirical constants α_m and β_m. A further investigation of the influence of these constants on r_h is recommended for future research in the comparison of MA, BO and RA methods.

Highest r_h values are found in all three approaches in a lot with high rise buildings left to the extended park area and in some parts of the very dense housing areas.

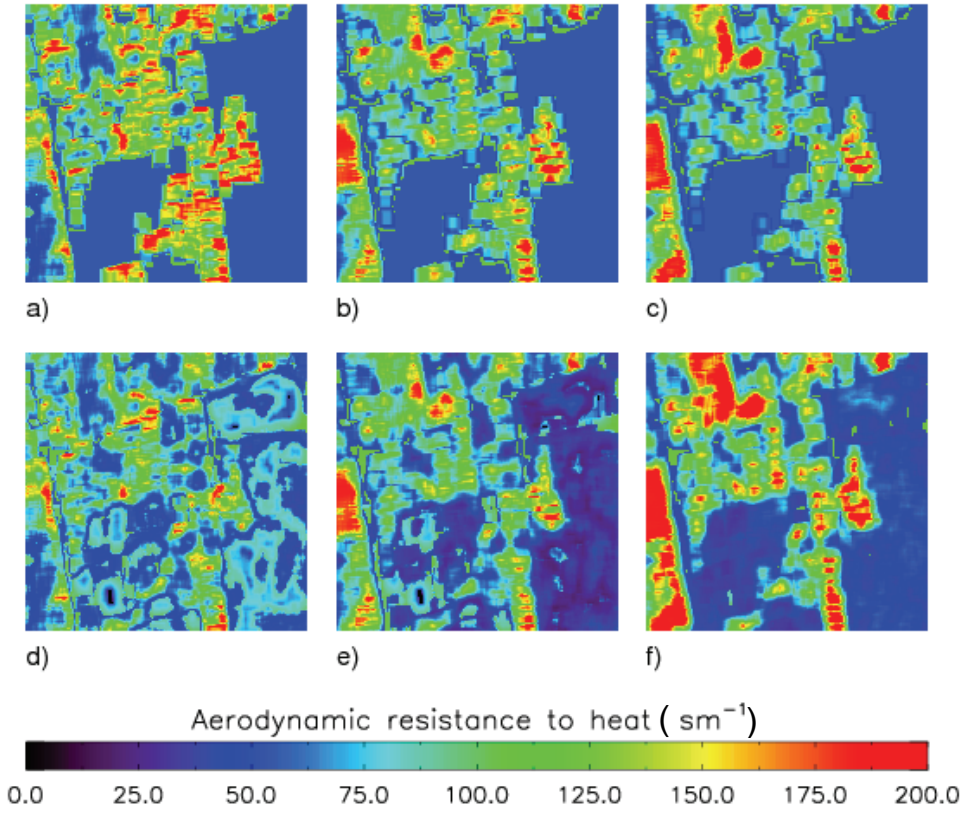

Figure 6: Aerodynamic resistance to heat, calculated with 125 m windows for a wind direction of 0°, for the MA (a + d), the BO (b + e) and the RA (c + f) approach. The upper line shows the first model, the lower line the second model, including assumptions about vegetation.

CONCLUSIONS

The use of morphometric methods for the estimation of the aerodynamic resistance to heat r_h is a promising approach when spatial data is needed. The precondition of a high resolution city model however, restricts this method to areas where such models are available. With the launch of TerraSAR-X and its twin TanDEM-X of the German Aerospace Center more and more high resolution DEMs will be available worldwide from about 2014. In this study a new city model was built from Spot and Google Earth images for the extent of the test area.

The mean density λ_p and the mean frontal area index λ_f were lower than literature values because of specific characteristics of the area and the surface model. Higher λ_p and λ_f values would result in a higher aerodynamic resistance.

Due to the semi-empiric nature of the estimation of the roughness lengths, it is necessary to define optimal parameters for urban surfaces. This study is an approach to find an optimal configuration of the morphometric methods to fit values deducted from *in situ* measurements. The best fitting α value was similar for the three different methods and the two surface models. The best fitting α values range from -0.5 to -0.7, independent of the wind speed. A value of -0.6 is recommended for further studies in this area.

A wind direction dependent comparison of *in situ* and modelled r_h values revealed that all three methods could reproduce the general directional pattern measured by *in situ* instrumentation induced by different surface roughness.

The spatial analysis finally showed that extended areas with no surface elements produce probably unrealistically values. It is therefore recommended to insert a minimum roughness in extended open areas. The inclusion of vegetation in the model also solved this problem. Generally high r_h

values are found in areas with a high roughness, which could be induced by high buildings or a higher building density. Only in some of the very high density areas the three methods did not agree in their results.

ACKNOWLEDGEMENTS

This work was supported by the Swiss National Science Foundation (grant number 200020–120080/1).

REFERENCES

1 Verma S B, 1989. Aerodynamic resistances to transfer of heat, mass and momentum in estimation of areal evaporation. IAHS Publication, 177: 13-20 (last date accessed: 14.12.2010)

2 Grimmond C S B & T R Oke, 1999. Aerodynamic properties of urban areas derived from analysis of surface form. Journal of Applied Meteorology, 38, 1262-1292

3 Bottema M, 1997. Urban roughness modelling in relation to pollutant dispersion. Atmospheric Environment, 31: 3059-3075

4 Raupach M R, 1994. Simplified expressions for vegetation roughness length and zero-plane displacement as functions of canopy height and area index. Boundary Layer Meteorology, 71: 211-216

5 Raupach M R, 1995. Corrigenda. Boundary Layer Meteorology, 76: 303-304

6 Macdonald R W, R F Griffiths & D J Hall, 1998. An improved method for the estimation of surface roughness of obstacle arrays. Atmospheric Environment, 32(11): 1857-1864

7 Liu G, J Sun & W Jiang, 2008. Observational verification of urban surface roughness parameters derived from morphological models. Meteorological Applications, DOI: 10.1002/met.109

8 Burian S J, J B Michael & S P Linger, 2002. Morphological analyses using 3D building databases: Los Angeles, California. Los Alamos National Laboratory, LA-UR-02-0781, 73 pp. (last date accessed: 14.12.2010)

9 Gál T & Z Sümeghy, 2007. Mapping the roughness parameters in a large urban area for urban climate applications. Acta Climatologica et Chorologica. Universitatis Szegediensis, Tomus 40-41: 27-36

10 Ratti C, S Di Sabatino, R Britter, M Brown, F Caton & S Burian, 2002. Analysis of 3-D urban databases with respect to pollution dispersion for a number of European and American cities. Water, Air and Soil Pollution: Focus 2(5-6): 459-469

11 Ioannilli M & E Rocchi, 2008.Urban roughness parameters calculation in the city of Rome by applying analytical and simplified formulations: Comparison of results. Lecture Notes in Computer Science, 5072: 284-299

12 Brutsaert W, 1982. Evaporation into the Atmosphere. Theory, History and Applications (Kluwer Academic Publishers, Dordrecht) 264 pp.

13 Kanda M, M Kanega, T Kawai, R Moriwaki & H Sugawara, 2007. Roughness lengths for momentum and heat derived from outdoor urban scale models. Journal of Applied Meteorology and Climatology, 46: 1067-1079

14 Kawai T, M K Ridwan & M Kanda, 2009: Evaluation of the simple urban energy balance model using selected data from a 1-yr flux observation at two cities. Journal of Applied Meteorology and Climatology, 48: 693-715

15 Loridan T, C S B Grimmond, S Grossman-Clarke, F Chen, M Tewari, K Manning, A Martilli, H Kusaka & M Best, 2010: Trade-offs and responsiveness of the single-layer urban canopy

parameterization in WRF: an offline evaluation using the MOSCEM optimization algorithm and field observations. Quarterly Journal of the Royal Meteorological Society, 136: 997-1019

16 Frey C M & E Parlow, 2010. Flux measurements in Cairo. Part 2: On the determination of the spatial radiation and energy balance using ASTER satellite data. International Journal of Climatology, submitted

17 Xu W, M J Wooster & C S B Grimmond, 2008. Modelling of urban sensible heat flux at multiple spatial scales: A demonstration using airborne hyperspectral imagery of Shanghai and a temperature–emissivity separation approach. Remote Sensing of Environment, 112: 3493-3510

18 Foken T, 2003. Angewandte Meteorologie (Berlin: Springer) 289 pp.

19 Chehbouni G, Y Nouvellon, J P Lhomme, C Watts, G Boulet, Y H Kerr, M S Moran & D C Goodrich, 2001. Estimation of surface sensible heat flux using dual angle observations of radiative surface temperature. Agriculture and Forest Meteorology, 108: 55-65

20 Voogt J A & C S B Grimmond, 2000. Modelling surface sensible heat flux using surface radiative temperatures in a simple urban area. Journal of Applied Meteorology, 39: 1679-1699

21 Goossens R, F M R Tack, D Devriendt, O Ateya & E Parlow, 2008. DEM-generation from SPOT 5 across-track imagery. A case study over CAIRO and surroundings. 28th EARSeL Symposium: Remote Sensing for a Changing Europe (EARSeL, Strasbourg)

22 Kormann R & F X Meixner, 2001. An analytic footprint model for neutral stratification. Boundary-Layer Meteorology, 99: 207-224

23 Frey C M, E Parlow, R Vogt, M Abdel Wahab & M Harhash, 2010. Flux measurements in Cairo. Part 1: In situ measurements and their applicability for comparison with satellite data. International Journal of Climatology, doi: 10.1002/joc.2140

24 Liu S, Lu L, Mao D, Jia L, 2007. Evaluating parameterizations of aerodynamic resistance to heat transfer using field measurements. Hydrology and Earth System Science, 11: 769-783